Synthetic data framework to estimate the minimum detectable concentration of contrast agents for multispectral optoacoustic imaging of small animals

Hong Yang [1,2], *Ivan Olefir* [1,2], *Stratis Tzoumas* [3], *Vasilis Ntziachristos* [1,2,*]

*Corresponding Author: E-mail: Vasilis Ntziachristos (v.ntziachristos@tum.de)

[1] Institute of Biological and Medical Imaging (IBMI), Helmholtz Zentrum München, Neuherberg, Germany
[2] Chair of Biological Imaging, TranslaTUM, Technical University of Munich, Munich, Germany
[3] Department of Radiation Oncology, School of Medicine, Stanford University, Stanford, USA

Keywords: optoacoustic/photoacoustic imaging, MDC, detection limit, molecular sensitivity, spectral unmixing.

Abstract

The concentrations of contrast agents for optoacoustic imaging of small animals must usually be optimized through extensive pilot experiments on a case-by-case basis. The present work describes a streamlined approach for determining the minimum detectable concentration (MDC) of a contrast agent given experimental conditions and imaging system parameters. The developed Synthetic Data Framework (SDF) allows estimation of MDCs of various contrast agents under different tissue conditions without extensive animal experiments. The SDF combines simulated optoacoustic signals from exogenously administered contrast agents with *in vivo* experimental signals from background tissue to generate realistic synthetic multispectral optoacoustic images. In this paper, the SDF is validated with *in vivo* measurements and demonstrates close agreement between SDF synthetic data and experimental data in terms of both image intensity and MDCs. Use of the SDF to estimate

This article has been accepted for publication and undergone full peer review but has not been through the copyediting, typesetting, pagination and proofreading process which may lead to differences between this version and the Version of Record. Please cite this article as doi: 10.1002/jbio.201900021

MDCs for fluorescent dyes and nanoparticles at different tissue depths and for imaging lesions of different sizes is illustrated.

1. Introduction

Contrast agents that absorb light can be imaged with high resolution using multispectral optoacoustic imaging through several millimeters to centimeters deep within tissue [1-3]. A number of studies have reported successful application of contrast agents in optoacoustic tomography, including fluorescent proteins [4]; fluorescent dyes such as IRDye800 [5], indocyanine green (ICG) [6] and Alexa Fluor 750 (AF750) [7]; carbon nanotubes [8]; polymer nanoparticles [9]; and gold nanorods (GNRs) [10]. The optimal concentration of these contrast agents for a given experimental situation and imaging set-up cannot currently be estimated in advance, which means that it must be determined through pilot studies that require time and effort and increase the number of experimental animals required. Such pilot studies could be minimized if an analytical method was available to estimate the minimum detectable concentration (MDC) for contrast agents under a given set of experimental conditions and imaging hardware specifications. Such a method could also help streamline efforts to design next-generation optoacoustic contrast agents.

The MDC of a contrast agent in multispectral optoacoustic imaging depends on a multitude of parameters: (1) characteristics of the contrast agent employed, i.e. the molar extinction coefficient, Grüneisen coefficient and the absorption spectrum; (2) the agent location within tissue (tissue depth); (3) the size of the lesion occupied by the agent; (4) the optical properties and overall characteristics of the imaged tissue; (5) the specifications of the imaging system

and (6) the image reconstruction and spectral analysis method used. Early efforts to identify the MDC of a contrast agent such as Cy5.5 in optoacoustic imaging was carried out with simulations and phantom experiments [11]. Although such studies offer insight into the physical parameters affecting the MDC, they typically focus on the characterization of the performance of the imaging systems and do not consider the challenges of *in vivo* small-animal imaging, in which the optoacoustic contrast agent is embedded in tissue and needs to be spectrally unmixed from a spatially heterogeneous absorbing tissue background. Therefore, the MDC values refer to the particular parameters contained in the simulation or phantom studied but do not universally capture *in vivo* conditions.

Detection limits in biological tissues (e.g. chicken muscle) *ex vivo* have also been considered for better approximation of tissue imaging conditions and for exploring the maximum imaging depth achieved using a certain agent concentration [5, 12]. However, excised muscle tissue does not reproduce the complex, dynamic physiological conditions that affect optoacoustic contrast *in vivo*, such as the hemoglobin distribution. Moreover, those previous studies did not consider multispectral detection. Reports of the detection of contrast agents *in vivo* have enabled insight into the MDCs of a few contrast agents in real settings but also do not allow for a generalized understanding of the MDC values achieved. As a result, it is not possible to extrapolate from those measurements in order to estimate MDCs if experimental parameters change, such as the applied contrast agent, tissue, depth, lesion size or imaging set-up.

Here we developed a streamlined approach to estimate the MDCs of exogenous contrast agents in small-animal optoacoustic imaging for a given set of experimental conditions and

imaging parameters, which may reduce the need for extensive animal experiments. We developed a Synthetic Data Framework (SDF) that combines experimental measurements and a signal simulation framework to derive synthetic multispectral optoacoustic images. Background optoacoustic signals are experimentally measured from animals *in vivo*, in the absence of exogenous agents. Using these measurements as the imaging background, SDF simulates the signals obtained from assumed agents embedded in tissue, enabling a framework that allows the generalized study of MDCs of contrast agents by achieving simulations that correspond to the optical properties and detection conditions of live animal tissues, and the specifications of a real optoacoustic imaging system. The SDF developed was validated using experimental *in vivo* data on tissue containing known concentrations of contrast agents. Image intensity and MDCs generated using the SDF agree closely with experimental data. Finally, we showcase the application of the SDF to estimate the MDCs of AF750 and GNRs in multispectral optoacoustic tomography for different conditions, such as lesion size and imaging depth.

2. Materials and Methods

2.1. Synthetic Data Framework (SDF): concept and approach

The SDF platform generates synthetic images that mimic multispectral optoacoustic experimental images: the tissue background is based on experimental data from healthy, untreated animals, while the signal from exogenous contrast agent is simulated based on the known properties of the agent, the estimated optical properties of background tissue and the specifications of the imaging system. The SDF simulator compensates for the fact that while it is straightforward to simulate the propagation of optoacoustic signals emitted from well-

defined agents, it is difficult to accurately simulate signals coming from tissue, since the optical and acoustic properties of biological tissues are not precisely known.

To develop a generalized way to study the MDCs of different agents under varied conditions, we developed a pipeline called the SDF, which comprises three modules (Figure 1). The input of the SDF is an assumed molar concentration distribution of a contrast agent in tissue and the wavelength-dependent molar extinction coefficient of the agent. The output of the SDF is a synthetic multispectral optoacoustic image stack.

The Simulation Module consists of the SDF simulator, which uses the semi-analytical solution of the optoacoustic wave equation [13] to compute the optoacoustic signals coming from the contrast agent input distribution. In the Agent Implantation Module, the simulated signals of the agent are superimposed onto the experimental signals of background tissue obtained from *in vivo* measurement of a mouse without any exogenous contrast agent. Then the synthetic signals are reconstructed to form synthetic optoacoustic images. In the Detection Module, the synthetic optoacoustic images are spectrally unmixed and a detection metric is applied to the unmixing result to determine the MDC of the agent.

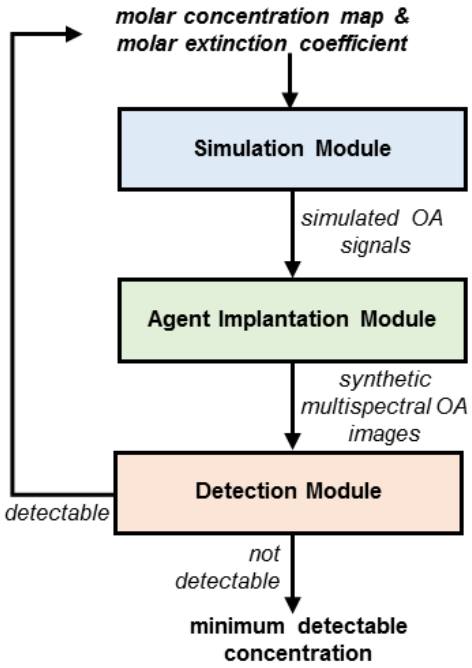

Figure 1. Schematic presentation of the SDF. The Simulation Module simulates the optoacoustic (OA) signals of a contrast agent. Then, the simulated signals are superimposed onto *in vivo* background signals in the Agent Implantation Module, thereby generating synthetic multispectral optoacoustic images. Finally, in the Detection Module, the synthetic images are analyzed to determine the detectability of the contrast agents and the MDCs.

2.2 Simulation Module: Simulation of optoacoustic signals of contrast agents

Figure 2 depicts the workflow in the SDF Simulation Module. This module simulates the detected optoacoustic signals of the exogenous contrast agent located inside tissue. In the simulation, we take into account three main factors involved in the optoacoustic signal formation [14]: (1) the light fluence at the agent location, (2) the propagation of pressure perturbations that arise when the tissue absorbs the laser light and heats up, and (3) the characteristics of the imaging system such as the spatial impulse response (SIR) and the

electrical impulse response (EIR) of the transducer array. In the first step of the Simulation Module, a molar concentration map $c(\mathbf{x})$ of an agent within tissue with absorption coefficient $\mu_a(\mathbf{x},\lambda) = c(\mathbf{x})\varepsilon(\lambda)$ is assumed, ε being the molar extinction coefficient. Assuming illumination by a transient light fluence field $/\ (\mathbf{x},\lambda)$, the initial pressure P_{init} is equivalent to:

$$P_{init}(\mathbf{x},\lambda) = \text{“} \cdot /\ (\mathbf{x},\lambda) \cdot \mu_a(\mathbf{x},\lambda), \tag{1}$$

where $\mathbf{x}$ is spatial coordinates, λ is the wavelength and “ is the Grüneisen coefficient. The propagating pressure waves P_w can be simulated as a function of the initial pressure distribution as:

$$P_w(\mathbf{x},\lambda) = \mathbf{M} \cdot P_{init}, \tag{2}$$

where $\mathbf{M}$ is a model matrix that corresponds to the geometry of the imaging system and describes the optoacoustic wave propagation in the imaging domain, as calculated analytically in [13]. To achieve a more accurate approximation of the spatially averaged pressure $P_{avg}(\mathbf{x},\lambda)$ on the active area of the transducer element, the SIR of the transducer array is also modeled in the present study. Each cylindrically focused transducer element of the transducer array is approximated by N line transducers (N=140 in this study), and the SIR of each line transducer is calculated analytically [15]. The above process can be noted mathematically as

$$P_{avg}(\mathbf{x},\lambda) = \mathrm{S}(\mathbf{M}) \cdot P_{init}, \tag{3}$$

where S stands for the operation that incorporates the SIR of the transducer array into model matrix $\mathbf{M}$.

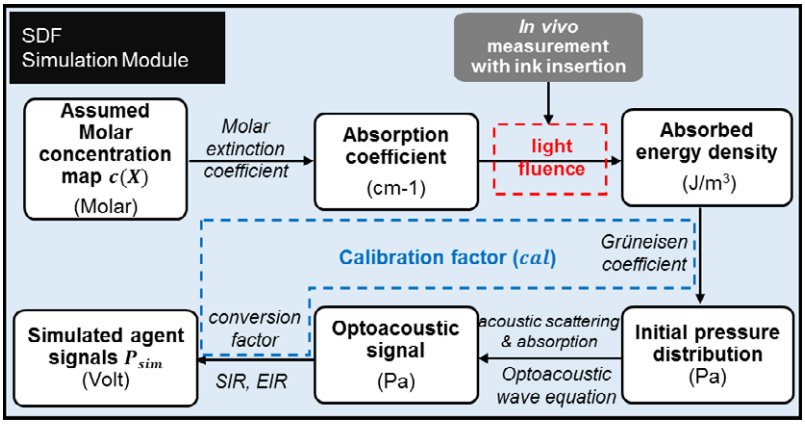

Figure 2. Detailed schematic of the SDF Simulation Module, which simulates the optoacoustic signals of contrast agents inside tissue. The dashed boxes identify parameters whose estimation is crucial for taking into account the specific properties of the tissue, the contrast agent and the transducer. These crucial parameters are explained in detail in the text. EIR, electrical impulse response; SIR, spatial impulse response; P_{sim}, optoacoustic signals of contrast agents simulated according to Equation (7).

Frequency-dependent acoustic attenuation of the optoacoustic waves (a combined effect of acoustic scattering and absorption) is simulated according to the following formula, which corresponds to a uniformly attenuating medium. The acoustic pressure P_{att} after attenuation can be expressed as

$$P_{att}(\mathbf{x},\lambda)=\mathrm{Re}\left\{F^{-1}(F(P_{avg})\cdot h_{att})\right\}, \tag{4}$$

where F and F^{-1} stand for the Fourier and inverse Fourier transforms, respectively; and $h_{att}(f,d)=\exp(-\alpha_{0f}|f|^{n}d)$ is the acoustic attenuation function [16], where α_{0f} is a material-related acoustic attenuation constant, n is a real positive constant, f is the frequency bandwidth of the agent and d is the propagation distance of the acoustic wave. For water,

α_{0f}=0.00217dB$\cdot$MHz$^{-2}\cdot$cm^{-1} and n is 2; for tissues, n is 1 and $\alpha_{0f} \approx 0.5$ dB$\cdot$MHz$^{-2}\cdot$cm^{-1} [17]. In the considered case, the distance d from the agent to the surface of the transducer is assumed to be constant at 4 cm (1 cm tissue and 3 cm water). The pressure signal $P_{\text{att}}(\mathbf{x},\lambda)$ reaching the transducer surface is converted into an electrical signal P as follows:

$$P(\mathbf{x},\lambda,t) = k \cdot h_{EIR}(\mathbf{x},t) * P_{\text{att}}(\mathbf{x},\lambda), \tag{5}$$

where $h_{EIR}(\mathbf{x},t)$ is the experimentally measured EIR of the transducer element and k is a constant for converting pressure to voltage. Combining Equation (1-5) allows the acquired pressure signals to be expressed as a function of the agent concentration:

$$P_{sim}(\mathbf{x},\lambda) = k \cdot h_{EIR} * \text{Re}\left\{F^{-1}(F(\Gamma \cdot \text{S}(\mathbf{M}) \cdot I^{/} \cdot c(\mathbf{x}) \cdot \varepsilon) \cdot h_{att})\right\}. \tag{6}$$

Equation (6) expresses the acquired optoacoustic signals as a function of the spatially varying agent concentration $c(\mathbf{x})$ through sequential steps graphically presented in Figure 2. Equation (6) includes three additional unknown parameters: the light fluence field $I^{/}$, which is strongly dependent on the background tissue; the Grüneisen coefficient Γ of the agent, which is typically not known; and the conversion factor k. The Grüneisen coefficient and conversion factor are jointly estimated as one calibration factor cal, which leads to a simplified form of Equation (6):

$$P_{sim}(\mathbf{x},\lambda) = cal \cdot h_{EIR} * \text{Re}\left\{F^{-1}(F(\text{S}(\mathbf{M}) \cdot I^{/} \cdot c(\mathbf{x}) \cdot \varepsilon) \cdot h_{att})\right\}, \tag{7}$$

where $cal = \Gamma \cdot k$. In order to generate realistic simulated signals, we derived the optical properties of background tissue for light fluence estimation based on the spectral coloring effect of a reference point inside the imaged tissue (see Supporting Information Section 1). The calibration factor cal of each contrast agent was measured in phantom experiments (see

Supporting Information Section 2).

2.3. Agent Implantation Module: Agent implantation

Figure 3 shows that the simulated optoacoustic signals P_{sim} (output of Simulation Module), which correspond to an assumed concentration distribution of an agent, are merged with experimentally measured background signals P_{exp} to produce synthetic signals P_{syn}. In other words,

$$P_{syn} = P_{sim} + P_{exp} . \tag{8}$$

In Equation (8), P_{exp} is the experimental signals obtained from *in vivo* experiments of a mouse without any exogenous contrast agent, and the synthetic signals P_{syn} are reconstructed to generate synthetic multispectral optoacoustic images. In this study, we reconstructed all images using a least squares minimization algorithm (LSQR) and standard Tikhonov regularization with a field of view (FOV) of 2×2 cm^2 and 200×200 pixels.

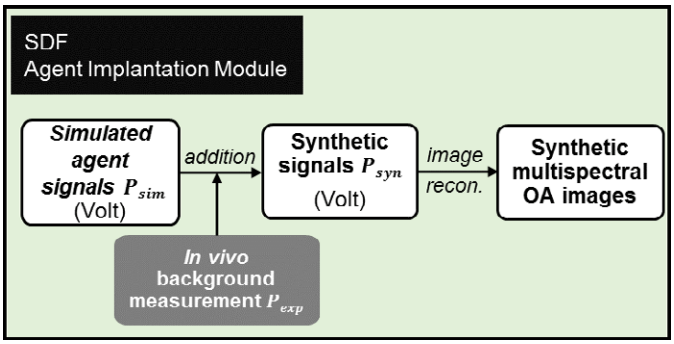

Figure 3. Schematic of agent implantation. The simulated optoacoustic signals of an agent (output of Simulation Module) are superimposed onto experimental tissue signals from an *in vivo* animal measurement, giving rise to synthetic optoacoustic signals. After image reconstruction, synthetic multispectral optoacoustic images are generated.

2.4. Detection Module: Agent detection

Figure 4 shows the derivation of MDC of a contrast agent in multispectral optoacoustic imaging based on the SDF simulator. To assess the MDC as a function of tissue depth, lesion size and contrast agent, we analyzed the reconstructed synthetic images produced by the Agent Implantation Module using an unmixing algorithm based on the Adaptive Matched Filter (AMF) [18]. Our goal was to spectrally resolve the distribution of the agent from the absorbing background. The spectral unmixing result is a 2D image $D(\mathbf{x})$. In order to derive the MDC of the agent, a standard for defining an agent as 'detectable' should be established. In the present study, the agent was treated as 'detectable' if it could be distinguished from the background with only a moderate amount of false positives after unmixing, which can be expressed as

$$\sum_{\mathbf{x}\in D_a} D(\mathbf{x}) > \sum_{\mathbf{x}\in D_b \wedge D(\mathbf{x})>\bar{T}} D(\mathbf{x}), \tag{9}$$

where D_a is the agent region and D_b is the background region, $D_b = D \setminus D_a$ and '\' denotes set subtraction, and $\bar{T}$ is the mean intensity of the agent region from the unmixing result D. According to the detection metric above, if the agent is detectable, the process restarts at the Simulation Module, this time with a lower input concentration. The iterations continue until the agent can no longer be detected. Then the lowest detectable concentration is defined as the MDC.

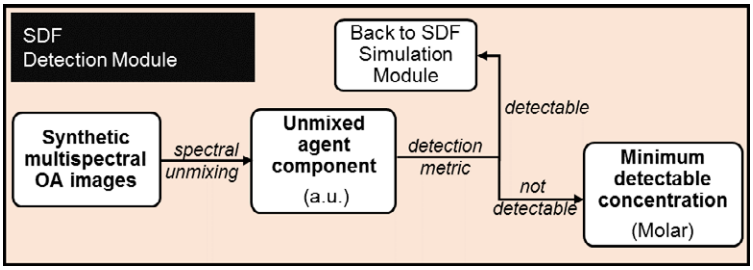

Figure 4 Schematic of the determination of a contrast agent's minimum detectable concentration in multispectral optoacoustic imaging. The synthetic multispectral optoacoustic images generated by SDF simulator are unmixed. Then a detection metric is applied to the unmixing result to define the detectability of the contrast agent until the MDC is defined.

2.5. SDF validation

To validate the SDF simulator, we performed experiments with two anesthetized CD1 mice *in vivo*, i.e. Group A and Group B in Table 1 using the commercially available inVision256 system (iThera Medical GmbH, Munich, Germany), which features a transducer array of 256 cylindrically focused elements providing 270° angular coverage; the transducer array has a radius of 40 mm and a central frequency of 5 MHz. For each animal experiment, a polyester capillary tube of inner diameter 0.8/1 mm was rectally inserted into the mouse. Then the mice were imaged in the lower abdominal area at 21 wavelengths (from 700 nm to 900 nm with 10-nm interval). First, the animal was scanned with a water-filled tube in order to acquire the background signals for agent implantation (Experiments A1 and B1). Then for Group A experiments, the inserted tube was iteratively filled with 2 concentrations of ink (4.6 and 9 cm^{-1}) (Experiment A2) and 10 increasing concentrations of AF750 (0.12, 0.21, 0.35, 0.64, 1.22, 2.3, 4.6, 9.2, 16.1 and 23 cm^{-1}) (Experiment A3). For Group B experiments, the inserted tube was iteratively filled with distilled water (Experiment B1), 8 concentrations of ink (0.35,

0.58, 0.78, 1.52, 3.54, 4.49, 5.75 and 8.74 cm^{-1}) (Experiment B2) and 8 increasing concentrations of AF750 (0.28, 0.64, 0.74, 1.33, 2.78, 4.6, 9.2 and 13.8 cm^{-1}) (Experiment B3). All animal procedures were approved by the Government of Upper Bavaria.

As a complement to the *in vivo* measurements in Experiments A2-3 and B2-3, we performed simulations using the SDF simulator, in which $\mu_a(\mathbf{x},\lambda)$ in the agent region equaled the absorption of agents used in the experiments *in vivo,* and the system specifications were the same as for the inVision 256 system. Four synthetic datasets were generated, Synthetic A2-3 and B2-3. To validate the simulation framework, the reconstructed synthetic images were compared to *in vivo* experimental images in two ways. First, the intensities of the agent region in synthetic and experimental optoacoustic images were compared in a process referred to below as 'intensity validation'. Second, the synthetic and experimental images were spectrally unmixed, and the minimum detectable AF750 concentrations determined from each set of images were compared. This process is referred to below as 'MDC validation'. Table 1 summarizes key information about *in vivo* experiments performed with inVision256 system in the present study.

Table 1. Summary of *in vivo* experiments

Group	Expt. no.	Agent	No. of concs.	Purpose
	1	none	0	Background signal for synthetic dataset
A	2	India ink	2	Light fluence field estimation; intensity validation
	3	AF750	10	Intensity validation; MDC validation
	1	none	0	Background signal for synthetic dataset
B	2	India	8	Light fluence field estimation;

	ink		intensity validation
3	AF750	8	Intensity validation; MDC validation

Expt. no., experiment number; No. of concs., number of concentrations

3. RESULTS

3.1. SDF validation

In order to validate the SDF, four synthetic datasets (Synthetic A2, A3, B2 and B3) were generated corresponding to Experiments A2, A3, B2 and B3 described in Section 2.5. We followed two approaches for validation to demonstrate the agreement of the SDF with the real experiments in terms of image intensity and MDC. In the first approach, the image intensity of the agent region in synthetic images was compared to that of the experimental ones; in the second approach, the MDC after spectral unmixing was compared.

3.1.1. Intensity validation

First we validated the accuracy of the SDF by comparing the image intensity within the agent area. Figure 5(a) - 5(e) correspond to the Group A experiments. Figure 5(a) presents the experimental background image from the abdominal area of the animal in Experiment A1; only the 750-nm image is shown for simplicity. Figure 5(b) presents the experimental image (in Experiment A3, highlighted as 'experimental' in all panels) in which the inserted tube containing AF750 at an absorption of 16.1 cm^{-1} is highlighted with a red circle. Figure 5(c) presents a synthetic image (highlighted as 'synthetic' in all figures) derived from the SDF simulator with the same absorption as Figure 5(b). Optoacoustic image intensities within the circled area for different concentrations of ink (Experiment A2 and Synthetic A2) and AF750 (Experiment A3 and Synthetic A3) are presented with blue error bars in Figure 5(d) and 5(e),

respectively.

Figure 5(f) - 5(j) correspond to the Group B experiments in Table 1. Figure 5(f) presents the background image from the abdominal area of the second animal in Experiment B1; only the 700-nm image is shown for simplicity. Figure 5(g) presents the image from Experiment B2 with the tube containing 5.7 cm^{-1} ink. Figure 5(h) is formed using the background signals shown in Figure 5(f) and the simulated signals of the ink region with the same absorption as in Figure 5(g). The optoacoustic image intensities within the circled tube area for different concentrations of ink (Experiment B2 and Synthetic B2) and AF750 (Experiment B3 and Synthetic B3) are presented, respectively, in Figure 5(i) and 5(j).

Group A

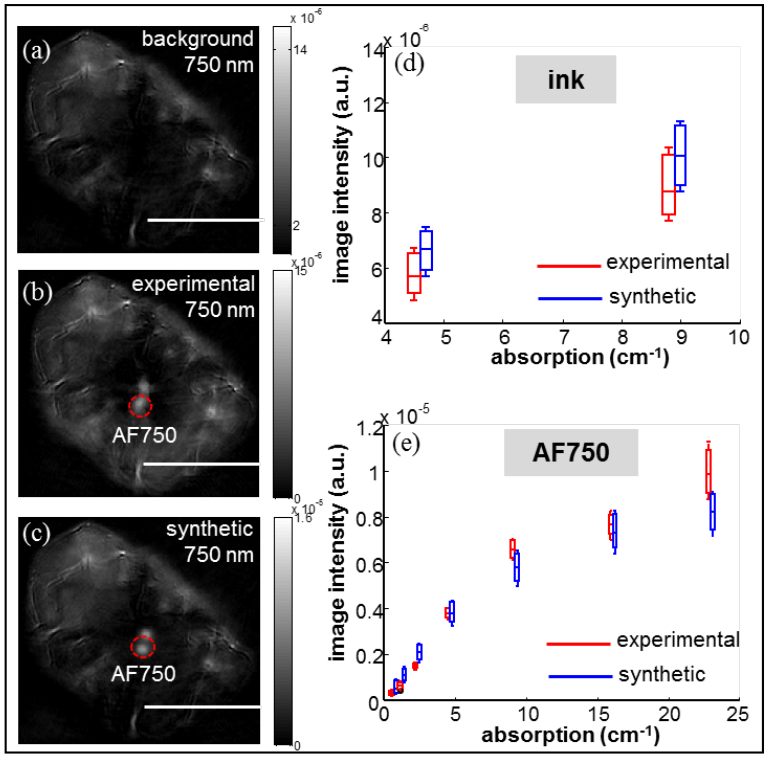

Group B

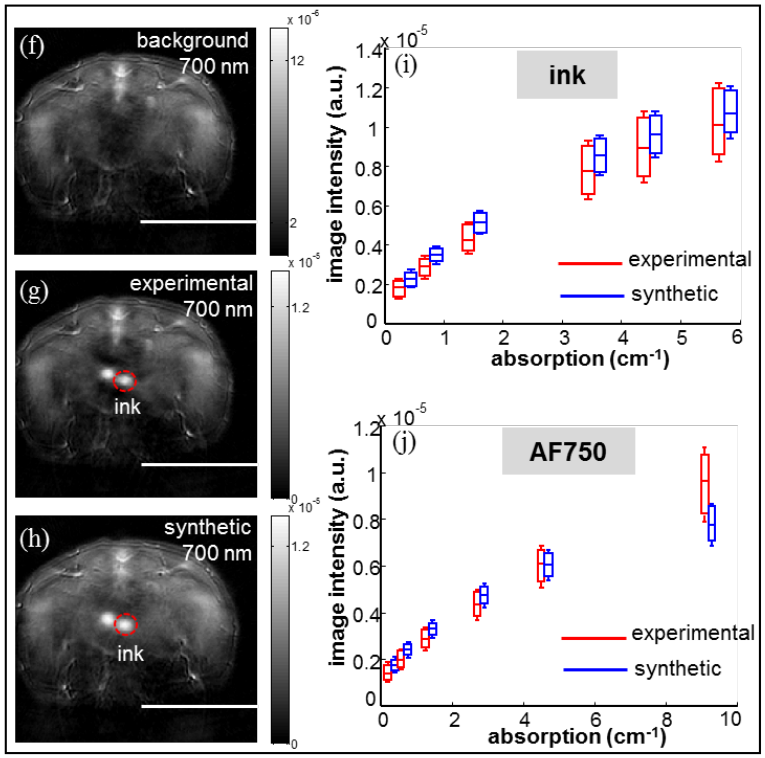

Figure 5. Comparison of the image intensity within the agent area between experimental and synthetic images. (a) Animal background image from Experiment A1; (b) experimental image with a 0.8-mm tube filled with 16.1 cm^{-1} AF750 at 750 nm (Experiment A3); (c) synthetic image with the simulated agent of the same absorption, location and size as the agent in panel (b); (d) quantitative analysis of image intensity within the agent area for Experiment A2 and Synthetic A2; (e) quantitative analysis of image intensity within agent area for Experiment A3 and Synthetic A3; (f) Group B animal background image (Experiment B1); (g) an experimental image of B2 with 1-mm tube filled with 5.75 cm^{-1} India ink at 700 nm; (h) synthetic image with the simulated agent of the same absorption, location and size as the agent in panel (g); (i) quantitative analysis of image intensity within agent area for Experiment B2 and Synthetic B2; (j) quantitative analysis of image intensity within agent area for Experiment B3 and Synthetic B3. All error bars stand for standard deviation. All scale bars are 1 cm.

From Figure 5(d), 5(e), 5(i), and 5(j), it can be seen that the mean and median intensities of the agent region agree well between experimental and synthetic optoacoustic images in most cases. Discrepancies in the intensity fluctuation range between experiments and simulations are due mainly to the manual segmentation of agent area in experimental images, which is unavoidable as there exists no prior information about the boundary of the agents' area.

3.1.2. MDC validation

Besides the intensity validation, we also applied spectral unmixing to the reconstructed images of Experiment A3, Synthetic A3, Experiment B3 and Synthetic B3 to verify the accuracy of the SDF. Figure 6(a) - 6(d) show the overlay of the spectral unmixing result of

AF750 (green) and anatomical optoacoustic image (gray) from Experiment and Synthetic A3 datasets at respective concentrations of 3.0 and 1.6 µM. Figure 6(e) - 6(h) are the spectral unmixing results of AF750 from Experiment and Synthetic B3 datasets at concentrations of 3.0 and 1.3 µM. Figure 6(a) and 6(b) show two adjacent concentrations in Experiment A3, and 6(e) and 6(f) show two adjacent concentrations in Experiment B3. Based on the detection metric in Equation (9), the agent in Figure 6(a) and 6(e) is detectable, while the agent in Figure 6(b) and 6(f) is not, which demonstrates that in this case the MDC of AF750 is about 3 µM. At the same time, the spectral unmixing results of corresponding synthetic datasets [Figure 6(c) - 6(d) and 6(g) - 6(h) also show the same MDC in both cases. Comparing these two groups of umixing results, it can be seen that the synthetic datasets provide the same MDC of AF750 as the experimental cases, which means that the SDF can determine MDC accurately.

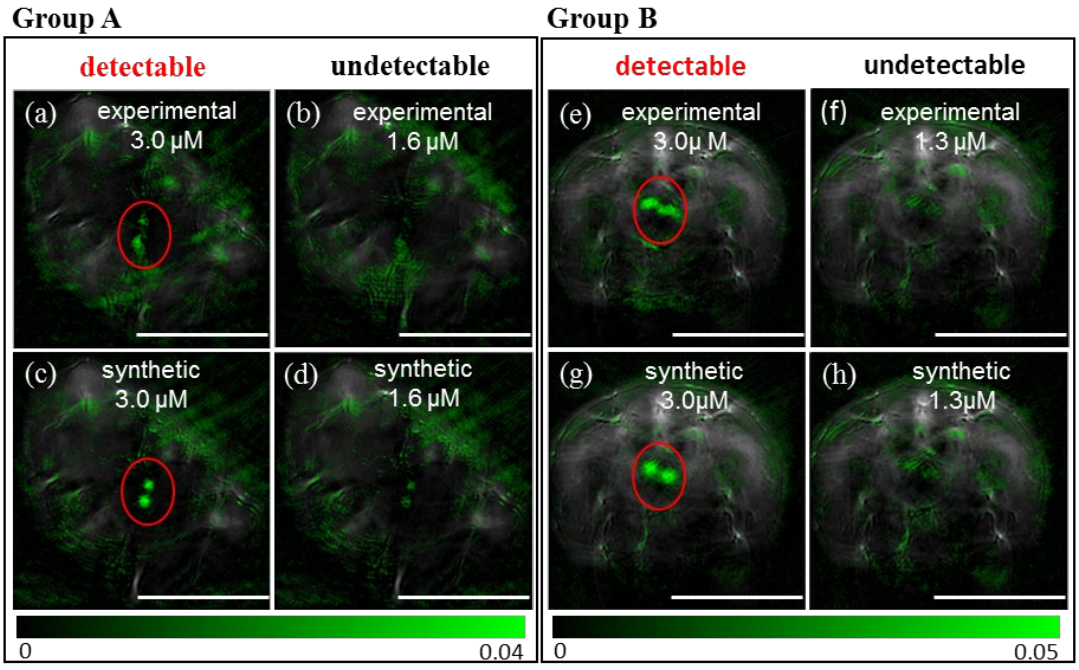

Figure 6. The MDC of AF750 after spectral unmixing in experimental and synthetic datasets. (a) Spectral unmixing result of Experiment A3 with 3.0 μM AF750; (b) spectral unmixing result of Experiment A3 with 1.6 μM AF750; (c) spectral unmixing result of Synthetic A3 at 3 μM; (d) spectral unmixing result of Synthetic A3 at 1.6 μM; (e) spectral unmixing result of Experiment B3 with 3 μM AF750; (f) spectral unmixing result of Experiment B3 with 1.3 μM AF750; (g) spectral unmixing result of Synthetic B3 with 3 μM AF750; (h) spectral unmixing result of Synthetic B3 with 1.3 μM AF750. All scale bars are 1 cm.

3.2. SDF-based MDC study

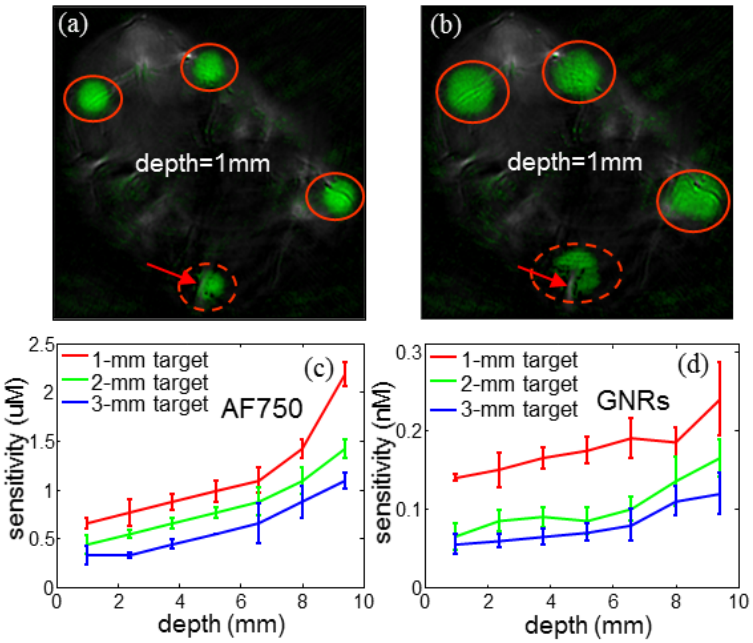

Figure 7. MDC curves of AF750 and GNRs as a function of depth with agents showing disk-like distributions with diameters of 1, 2 or 3 mm. (a) Spectral unmixing result for an agent with diameter of 2 mm at a depth of 1 mm; (b) spectral unmixing result for an agent with diameter of 3 mm at a depth of 1 mm; (c) MDCs of AF750 as a function of imaging depth for agents with diameters of 1, 2 or 3 mm; (d) MDCs of GNRs as a function of imaging depth for

agents with diameters of 1, 2 or 3 mm. All error bars show standard deviation.

After the validation of the SDF, various agents were implanted at different depths and volumes into Experiment A1 background signals [experimental signals corresponding to Figure 5(a)], and the MDC in each case was determined. Agents with distributions like disks with diameters of 1, 2 or 3 mm were separately implanted at seven imaging depths (1, 2.4, 3.8, 5.2, 6.6, 8 and 9.4 mm). At each imaging depth, 4 disks of the same diameter were implanted at different locations on the background to study the variations of the MDC at the same imaging depth; such variations should reflect mainly heterogeneity in the background. Figure 7(a) and 7(b) show that 4 agents with diameters of 2 and 3 mm, respectively, are detected at a depth of 1 mm. Figure 7(c) and 7(d) are the MDC curves of AF750 and GNRs, respectively. Both panels show that the MDC increases with depth of the agent and decreases with agent size. For each agent size, MDC of AF750 and GNRs varies at every depth, reflecting the heterogeneity of background tissue. For example, in Figure 7(a) and 7(b), four agents on the same image are of the same depth and size, but the agent on the bottom is much more difficult to detect than the other three agents. In other words, with the same depth and lesion size, the MDC of the bottom agent is much higher than the other three agents, which introduces standard deviation into the curve. Agent at the bottom was difficult to detect because of the strongly absorbing vessel (highlighted with a red arrow on the images) and the 270-degree transducer coverage. Since the synthetic signal P_{syn} is generated by superimposing the simulated optoacoustic signal of the contrast agent P_{sim} onto the experimental background signal P_{exp}, i.e. $P_{syn} = P_{sim} + P_{exp}$, the presence of a strong non-homogeneous intrinsic absorber such as blood vessels in the background means that the

background signal dominates the synthetic signal. In this case, the unmixing algorithm detects the main absorber at that location as hemoglobin and fails to detect the contrast agent. Additionally, the coverage angle of the transducer array is only 270 degrees and does not cover the central bottom part of the image. Therefore, signal from that region is slightly weaker than the signal from other regions. The MDC curve also fluctuates because the detection metric [shown in Equation (9)] is related to agent location and size. Comparing panel 7(c) and 7(d), we can see that GNRs can be detected with nanomolar MDC, which is much higher than micromolar MDC of AF750 in optoacoustic tomography.

4. Discussion

In this study, an SDF is developed to take into account experimental conditions and imaging set-up parameters in order to estimate the MDC of a given contrast agent for use in small-animal multispectral optoacoustic imaging. The synthetic data generated using this technique are compared against controlled *in vivo* experiments and show good agreement. For the first time, a framework can predict the MDCs of different contrast agents in varied conditions as a function of lesion size, imaging depth and agent type. The SDF may substantially streamline the currently tedious and animal-intensive process of optimizing contrast agent use in pre-clinical and basic optoacoustic imaging. It also provides a rational basis for assessing and comparing contrast agent performance under different conditions, and for comparing optoacoustic imaging systems.

The SDF developed in this study is able to generate realistic synthetic multispectral optoacoustic data mainly because it uses experimental measurements for tissue background signal and a calibrated agent implantation method. The concept of agent implantation has

previously been used [18, 19] to compare the performance of different spectral unmixing algorithms. However, in those previous studies, only the relative agent intensity was of interest, and therefore, the intensity of the implanted agents was not accurate in an absolute sense. That work was substantially expanded in the present study because we included a number of additional system parameters (SIR, EIR), physical effects (ultrasound attenuation) and calibration parameters (light fluence, Grüneisen coefficient) into our simulation in order to achieve accurate simulated agent intensities. Furthermore, instead of superimposing the image of simulated agents onto the background tissue image, we merged the simulated optoacoustic signals of agents with the experimental signals of background tissue before image reconstruction. This operation generates more realistic synthetic optoacoustic images by including the effect of reconstruction algorithms.

The SDF-predicted MDC values for our multispectral optoacoustic tomography system are comparable to values previously reported for dyes and GNRs using similar imaging set-ups. The results of the SDF-based MDC study indicate that the MDC of AF750 with inVision 256 system lies in the lower micromolar (< 2 μM) to upper nanomolar (> 200 nM) scale, depending on the agent size and imaging depth. In contrast, in the case of GNRs, the MDC values lie in the range of 200 pM to 50 pM. Although the reported MDCs of different contrast agents in optoacoustic tomography vary substantially across *in vivo* studies, similar MDC scales have been achieved in studies performed with dyes and gold nanoparticles in small-animal optoacoustic imaging (see Supporting Information Table S1).

As the MDC values predicted by the SDF-based study appear consistent with physical experiments, these numbers can be used as a reference for the minimum amount of contrast

agent that should be injected in multispectral optoacoustic studies or for the development of optoacoustic contrast agents. The SDF can also be used for optoacoustic imaging system design and analysis. For example, the influence of each factor (e.g. system hardware components, spectral unmixing algorithm, signal processing and imaging processing method) in attaining certain MDCs in multispectral optoacoustic imaging can be quantitatively analyzed using this simulation framework, since all those factors are independent and easily adjustable in the SDF. To explore parameter space through physical experiments would require significant time and effort and substantial numbers of experimental animals. Besides, the SDF might be useful to explore the application of different combination of dyes or nanoparticles with different sizes in optoacoustic imaging. The SDF-based MDC study comprises two stages: in stage 1, the SDF generates synthetic multispectral optoacoustic images; and in stage 2, spectral unmixing is applied to the synthetic multispectral optoacoustic image to detect the contrast agent and derive its MDC. In stage 1, the SDF can faithfully simulate optoacoustic images with any combination of dyes or nanoparticles if no particle aggregation occurs. However, in stage 2, in order to successfully detect the existence of two (or more) components in the mixture and determine their MDCs, some requirements need to be met: (1) the components in the mixture should be independent, which means that they do not chemically react with each other; (2) each component of the mixture should have sufficiently different absorption spectra to ensure adequate unmixing; and (3) the components in the mixture should generate optoacoustic signal of comparable intensity to ensure that strong signal due to one component does not "wash out" signal due to another.

Although the SDF-based MDC study is here validated and showcased based on a

commercial multispectral optoacoustic tomography system, the framework could also be used to identify MDCs of contrast agents for other state-of-the-art optoacoustic imaging systems and future applications. Meanwhile, the SDF is also suitable for (pre)clinical studies with various tissue types, such as hypoxic tissue. In this case, the oxygen saturation (sO_2) needs to be changed during the estimation of light fluence in the Simulation Module.

The SDF developed in this paper is designed mainly for cases where particle aggregation can be assumed not to occur in the applied contrast agent solution or suspension. Based on this, the SDF framework is applicable for dye solutions whose concentration is lower than 0.01 mM, since dimers become more significant when the concentration of the dye exceeds 0.01 mM [20]. The nanoparticle used in this study is gold nanorods (Ntracker™ from Nanopartz, D12M-780-50) of diameter 10 nm and of length 38 nm, which is guaranteed not to aggregate below 100 nM by the manufacturer. Since the aggregation behavior and absorbance of nanoparticles/their suspensions are highly dependent on the shape, size, structure, chemical composition and surface coatings of the utilized nanoparticles [21], case by case analysis might be inevitable for different nanoparticles.

In this study, the ink insertion was used as a reference point for the estimation of light fluence within tissue and for validation purposes. However, other ways to get the reference point are possible, for example by injecting a reference contrast agent or using an intrinsic absorber as the reference point. In addition, more accurate light fluence models and unmixing methods should be developed to deal with cases in which larger lesions are labeled with contrast agent.

5. Conclusion

We have developed a novel simulation framework that takes into account most effects in small-animal multispectral optoacoustic imaging, and its accuracy is demonstrated through *in vivo* experiments. Using this framework, we estimate the MDC of fluorescent dyes (AF750) and GNRs as a function of agent size and imaging depth based on the system parameters of a commercially available multispectral optoacoustic tomography system. With this method, the MDCs of various contrast agents can be systematically predicted as a function of experimental conditions and imaging set-up in order to optimize the type and concentration applied for multispectral optoacoustic studies. This can save time and resources as well as improve animal welfare by offering greater insight during the experimental design stage. This framework can guide the development and optimization of next-generation optoacoustic contrast agents, and it will be useful as a tool to study the effect of each parameter in Equation (7) on the MDC values, which will allow systematic studies to improve and compare the performance of multispectral optoacoustic imaging systems.

ACKNOWLEDGMENT

The research leading to these results has received funding from the Deutsche Forschungsgemeinschaft (DFG) [Cluster of Excellence "Nanosystems Initiative Munich (NIM)" and Gottfried Wilhelm Leibniz Prize 2013 (NT 3/10-1)] and from the European Research Council (ERC) under the European Union's Horizon 2020 research and innovation programme under grant agreement no. 694968 (PREMSOT). H. Yang acknowledges the support of a CSC fellowship (CSC No. 201506960010).

We thank A. Chapin Rodríguez, PhD, JP Fuenzalida, PhD, and Yuanhui Huang for helpful suggestions on the manuscript, and Sarah Glasl for technical assistance.

REFERENCES

[1] V. Ntziachristos, D. Razansky *Chemical reviews*. **2010**, *110*, 2783-2794.
[2] J. Weber, P. C. Beard, S. E. Bohndiek *Nature Methods*. **2016**, *13*, 639.
[3] G. P. Luke, D. Yeager, S. Y. Emelianov *Annals of Biomedical Engineering*. **2012**, *40*, 422-437.
[4] N. C. Deliolanis, A. Ale, S. Morscher, N. C. Burton, K. Schaefer, K. Radrich, D. Razansky, V. Ntziachristos *Molecular Imaging and Biology*. **2014**, *16*, 652-660.
[5] M. Li, J. Oh, X. Xie, G. Ku, W. Wang, C. Li, G. Lungu, G. Stoica, L. V. Wang *Proceedings of the IEEE*. **2008**, *96*, 481-489.
[6] R. Nagaoka, T. Tabata, S. Yoshizawa, S.-i. Umemura, Y. Saijo *Photoacoustics*. **2018**, *9*, 39-48.
[7] D. Razansky, C. Vinegoni, V. Ntziachristos *Optics letters*. **2007**, *32*, 2891-2893.
[8] A. De La Zerda, C. Zavaleta, S. Keren, S. Vaithilingam, S. Bodapati, Z. Liu, J. Levi, B. R. Smith, T.-J. Ma, O. Oralkan *Nature nanotechnology*. **2008**, *3*, 557-562.
[9] J. V. Jokerst, D. Van de Sompel, S. E. Bohndiek, S. S. Gambhir *Photoacoustics*. **2014**, *2*, 119-127.
[10] J. V. Jokerst, A. J. Cole, D. Van de Sompel, S. S. Gambhir *ACS nano*. **2012**, *6*, 10366-10377.
[11] D. Razansky, J. Baeten, V. Ntziachristos *Medical physics*. **2009**, *36*, 939-945.
[12] A. Hariri, J. Lemaster, J. Wang, A. S. Jeevarathinam, D. L. Chao, J. V. Jokerst *Photoacoustics*. **2018**, *9*, 10-20.
[13] A. Rosenthal, D. Razansky, V. Ntziachristos *IEEE transactions on medical imaging*. **2010**, *29*, 1275-1285.
[14] B. Cox, J. G. Laufer, S. R. Arridge, P. C. Beard *Journal of biomedical optics*. **2012**, *17*, 0612021-06120222.
[15] D. Queirós, X. L. Déan-Ben, A. Buehler, D. Razansky, A. Rosenthal, V. Ntziachristos *Journal of biomedical optics*. **2013**, *18*, 076014-076014.
[16] X. L. Deán-Ben, D. Razansky, V. Ntziachristos *Physics in medicine and biology*. **2011**, *56*, 6129.
[17] T. L. Szabo, Diagnostic ultrasound imaging: inside out, Academic Press, **2004**.
[18] S. Tzoumas, N. Deliolanis, S. Morscher, V. Ntziachristos *IEEE Transactions on Medical Imaging*. **2014**, *33*, 48-60.
[19] S. Tzoumas, A. Nunes, N. C. Deliolanis, V. Ntziachristos *Journal of biophotonics*. **2015**, *8*, 629-637.
[20] J. Kunzler, L. Samha, R. Zhang, H. Samha *Am. J. Undergrad. Res*. **2011**, *9*, 1-4.
[21] E. M. Hotze, T. Phenrat, G. V. Lowry *Journal of environmental quality*. **2010**, *39*, 1909-1924.